# Outer Detector Efficiencies and Muon Tracking at KamLAND

by
Roger Alexandre Wendell

A thesis submitted to the faculty of the University of North Carolina at Chapel Hill in partial fulfillment of the requirements for the degree of Master of Science in the Department of Physics & Astronomy.

Chapel Hill
2004

Approved:

Hugon J. Karwowski, Advisor

Ryan M. Rohm, Reader

Arthur E. Champagne, Reader

**ABSTRACT**

ROGER ALEXANDRE WENDELL: Outer Detector Efficiencies and Muon Tracking at KamLAND

(Under the Direction of Hugon J. Karwowski)

Sensitive measurements at the Kamioka Liquid Scintillator Anti-Neutrino Detector (KamLAND) require strong reductions in backgrounds from muon sources. With recent failures of veto (outer) detector components, several issues concerning the detector's background reduction ability have been raised. To this end, we study KamLAND's veto detection efficiency using Monte Carlo simulations for several failure scenarios and compare them against estimations computed from real data. Recent results suggest high efficiencies for all but the most drastic scenarios considered. Further, we present work on the development of a veto detector based muon tracking algorithm to complement existing fitting routines which are independent of the veto system.

# ACKNOWLEDGMENTS

For any great work there are generally many influences surrounding the artist that have enabled his success. Though I cannot claim this work is great, nor that I am an artist, there are many upon whom I have relied to keep my sanity. My feeling is that when reading a thesis of any sort, people are really only interested in reading the acknowledgements (as you are now doing), so in the interest of entertaining and giving credit where credit is due, the only art in this work occurs right now.

The first rule of the acknowledgements section is: You DO NOT talk about Fight Club. Instead, talk about In-n-Out Burger, home of double-double animal style relief. Talk about duping casino waitresses into comping you drink after drink by pretending to gamble with a single nickel (and promptly cashing out). Talk about a left handed reverse layup over biophysicists, string theorists, or nuclear-condensed matter-material scientists. Talk about Japanese coffee. Talk about how a more exhaustive and entertaining list will be found in another future publication. More specifically, thanks to KCH for wasting my life. Hats off to the french: awwww peep. Thanks to Get Low on pocket aces on the river. Thanks to adopted parenting. Thanks to 'Love you mean it.' Thanks to real parenting. Most importantly, thanks to tctiteubelcf.

-r$\forall$w

April 2003

Dedicated to Fudd

# CONTENTS

# LIST OF FIGURES

# LIST OF TABLES

# Chapter 1

# Introduction

As the reader begins perusing this manuscript, there are $10^{15}\ cm^{-2}$ neutrinos pouring through their body every second. Since their presence goes largely undetected many wonder about the utility in studying them. Ironically, it is their rare interactions that make them a valuable tool for studying nuclear processes, as many of their kinematic properties upon detection will be the same as they were at the particle's birth.

Of chief interest since the 1960's has been studies of solar models which offer predictions of the neutrino flux at the Earth's surface produced by the many nuclear reactions throughout the star's interior. However, measurements of this flux have consistently observed a deficit, amounting to roughly one third of predictions. These discrepancies are compelling since they are not easily resolved by changes to the Standard Solar Model and imply that a revision to our understanding of physics is necessary. This difficulty has come to be known as the Solar Neutrino Problem.

A simple and elegant solution to the problem lies in the suggestion that neutrinos have mass which enables them to oscillate from one type into another. Although the suggestion is straightforward, its consequences are far reaching; neutrinos are massless in the otherwise successful Standard Model of particle physics. Nevertheless, the Super Kamiokande experiment gave convincing evidence for neutrino oscillation[Fuk98],

which was reinforced by the Sudbury Neutrino experiment four years later[Ahm02]. The oscillation mechanism, however, remained unclear.

It was at this point in 2002 that Kamioka Liquid Scintillator AntiNeutrino Detector (KamLAND) first began taking data to search for neutrino oscillations in a region known as the Large Mixing Angle solution (LMA) to the solar neutrino anomaly. At a depth of 2700 m.w.e beneath the mountains of Japan, KamLAND measures the antineutrino flux from nearby nuclear reactors and compares it against the expected flux calculated from known reactor fission rates to achieve a high sensitivity, low background probe of the LMA.

The purpose of the present work is to examine the veto portion of the detector responsible for reducing muon induced backgrounds in KamLAND's antineutrino measurements. Since the muon flux at the Kamioka site is well known [Hir88], Monte Carlo studies can be made to accurately model the detector's response. In Chapter Three of this Thesis, we consider a Monte Carlo study on the muon tagging efficiency of the veto detector and compare it with efficiencies calculated from real data. Chapter Four brings us one step closer to a precise comparison of the real calculations with a discussion of the development of a veto detector based muon tracking algorithm to complement one already in place for the main part of KamLAND. Finally we consider how this research may be used in conjunction with other muon background efforts from the KamLAND collaboration to improve the experimental results. At present though, we move into more detail on KamLAND and its physics.

# Chapter 2

# KamLAND and Physics

## 2.1 Detector Location and Geometry

KamLAND is located near Toyama, Japan in the Kamioka-Mozumi zinc mine beneath Mount Ikenoyama in the cavity of the former Kamiokande experiment. This location is particularly ideal since the work done during Kamiokande furnishes KamLAND with the cosmic ray muon spectrum at the site, which averages 0.34 Hz in the detector volume. Furthermore, the site is situated on average 180 km from KamLAND's target nuclear reactors, enabling KamLAND to make a long baseline observation of neutrino oscillation.

KamLAND itself is divided into two distinct cylindrically symmetric regions. The outer (or veto) detector (OD) is a right cylinder 20 m in height with a 10 m radius. At the center of the OD is the inner detector (ID), which is housed in an 18 m diameter stainless steel sphere, connected to the ceiling of the OD by a cylindrical chimney and supported by steel legs based at the bottom of KamLAND.

The OD is a water Čerenkov muon veto detector, filled with 3.2 kt of pure water, and 225 refurbished photomultiplier tubes (PMTs) taken from the Kamiokande experiment. To maximize the amount of light reaching the phototubes, the outer surface of the ID as well as the inner surface of the OD is covered with Tyvek, a

material renowned for its position independent reflective properties. Tyvek is also placed horizontally throughout the outer detector at 2 m below the ceiling and 2 m above the floor, dividing the space of the OD into three physical regions. The middle region is further divided, though not physically, at the sphere's equator for analysis purposes. In descending order from the vertical, these regions are referred to as (Top, Upper, Lower, Bottom)[1]. TUNL's main responsibility at KamLAND is the OD. See Figure 1.1.

In a similar fashion, a 13 m diameter balloon divides the inner detector into two regions. This balloon is 135 $\mu$m thick and is filled with one kiloton of pure liquid scintillator, a mixture of alkyl and aromatic organic molecules. It is here that KamLAND makes its measurements of antineutrino flux. To maintain its shape, the balloon is bound in Kevlar ropes suspended from the ID chimney, and also immersed in a mixture of mineral and isoparaffin oils (referred to as the buffer oil). Looking in on the balloon are 1879 PMTs responsible for the detection of Čerenkov light in the buffer oil, and scintillation from the heart of the detector.

## 2.2 Inner Detector Physics

KamLAND principally searches for a deficit in the antineutrino flux from surrounding nuclear reactors for evidence of neutrino oscillation. Oscillation refers to a neutrino or antineutrino spontaneously changing its flavor from one of three possible types (muon, electron, or tau), into a different one. These flavor designations arise from the context in which a the neutrino is created. For instance, neutrinos produced from weak boson decays in conjunction with the $\tau^+$ lepton are designated $\nu_\tau$, and their antiparticles are denoted with an overbar, $\overline{\nu_\tau}$. That this is possible when neutrinos have mass is roughly the statement that the flavor eigenstates are not the same as neutrino mass eigenstates. Then, in the same way that quarks are allowed to mix in

[1] all multiplets of this type will be given in this order throughout this paper

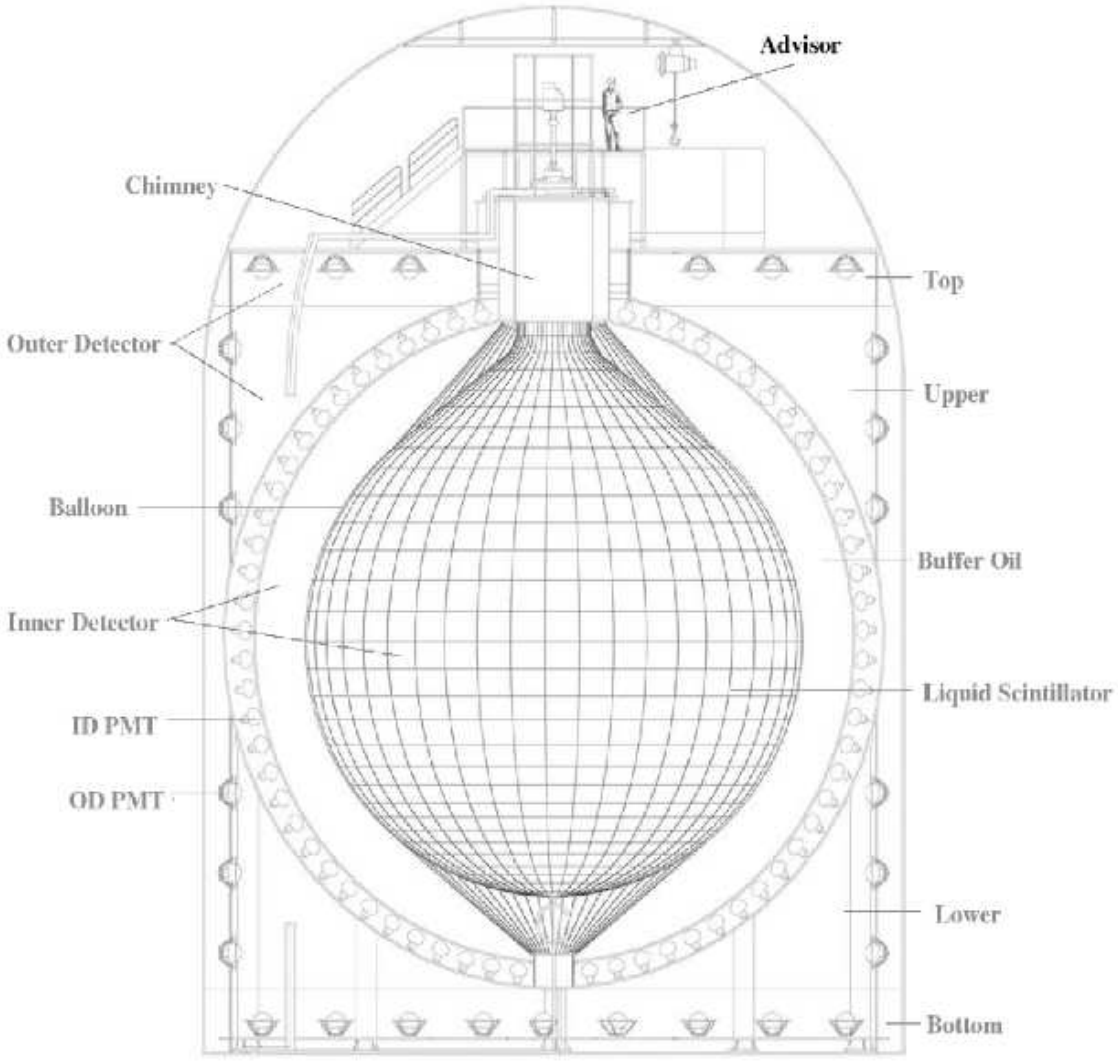


Figure 2.1: Cross sectional view of KamLAND

weak interaction physics, we create a unitary mass mixing matrix $U_{f,m}$ for neutrinos. A neutrino of flavor $f$ can then be represented as:

$$|\nu_f\rangle = \sum_m U_{f,m}|\nu_m\rangle, \tag{2.1}$$

where the sum on $m$ runs over mass eigenstates.

As such a superposition, neutrino oscillation is just a consequence of time evolution,

$$|\nu_j\rangle_t = e^{-iE_j t}|\nu_j\rangle_{t=0}, \tag{2.2}$$

where $E_j$ labels the energy of the $j^{th}$ eigenstate. For our purposes, the neutrinos are relativistic and this energy may be written $E_j = \sqrt{p_j^2 + m_j^2}$. Current best measurements suggest that the mass of the neutrino is much less than the energy, and assuming all the mass eigenstates have the same momentum $p_j = p$, we can expand the root as $E_j \approx p + \frac{m_j^2}{2p}$. At distances $l$ for which $t \approx l$, the probability of observing a neutrino of flavor $f$, from one of flavor $g$ is

$$P(\nu_g \to \nu_f) = |\langle \nu_f | \nu_g \rangle|^2 = | \sum_i U_{f,j}^* e^{-i(p + \frac{m_j^2}{2p})l} U_{g,j} \ |^2 \ . \tag{2.3}$$

It is most illuminating to consider a two neutrino oscillation scenario $\nu_e \leftrightarrow \nu_\tau$, with two mass eigenstates. Since the mixing matrix is now two dimensional and unitary we may write its elements in terms of a single angle:

$$U = \begin{pmatrix} cos\theta & sin\theta \\ -sin\theta & cos\theta \end{pmatrix}. \tag{2.4}$$

For our relativistic particles the total energy (not $E_j$) is approximately the momentum [2]. Plugging this and our mixing matrix into the above, the probability for oscillation from $\nu_e \to \nu_\tau$ becomes:

$$P(\nu_e \to \nu_\tau) = sin^2(2\theta) sin^2(\frac{1.27\delta_m^2 l}{E}). \tag{2.5}$$

In this formula the mass difference squared $\delta_m^2 = m_2^2 - m_1^2$ is measured in eV$^2$, $l$ in meters, and $E$ in MeV. This gives an oscillation length of

$$L_{osc} \approx \frac{2.48E}{\delta_m^2}[m]. \tag{2.6}$$

There are a few points of interest stemming from Equation 2.5. First, note that the oscillations are dependent on mass differences squared, not on individual masses, a feature which extends to mixing in more than two channels [Kay00]. Also, the

[2] actually this is not quite correct, but can be shown through a covariant treatment to have no overall effect on the oscillation probability [Giu03]

mixing angle $\theta$ above is a free parameter since the baseline $l$ is the known distance to the experiment from the reactors under consideration. Consequently, oscillation experiments probe regions in space formed by these parameters, and are not themselves sensitive to individual neutrino masses. KamLAND is sensitive to a section known as the Large Mixing Angle solution to the Solar Neutrino Problem with $(\delta^2_m, sin^2(2\theta)) = (1.8 \times 10^{-5} eV^2, 0.76)$ [Bah98]. The range of parameters accessible to KamLAND may be calculated using the reactor baselines and neutrino energies from $1.8 - 8$ MeV in Equation 2.6. Figure 2.2 shows a plot of various oscillation regions, including that to which KamLAND is sensitive and the LMA.

KamLAND observes the inverse beta decay process $\overline{\nu_e} + p \rightarrow n + e^+$ in its search for these oscillations. Two light signals come from this reaction, one prompt and one delayed, enabling an accurate separation of real neutrino events from other backgrounds. During the positron's travel through the scintillator it excites molecules which radiate light into the phototubes of the ID. The prompt signal is observed when the positron annihilates on an electron producing two more gamma rays. In total, the energy collected by the PMTs will be 1.02 MeV, plus the initial positron energy. When the neutron captures on a proton, a deuteron is produced along with a 2.2 MeV gamma ray as the delayed signal. From these signals the energy of the antineutrino can be reconstructed with a lower bound of 1.8 MeV. During data analysis, cuts are made on the gamma energies at $1.0 \leq E \leq 8.0$ MeV and $1.8 \leq E \leq 2.7$ MeV for the prompt and delayed signal, the later being cut on times 660 $\mu$s after the prompt event.

Though inverse beta decay is distinguishable, the scintillation of the positron is not a unique process. Any charged particle in the ID will scintillate, and may produce much more light than the positron of interest. At KamLAND, through going muons for instance, are capable of saturating the ID and blinding it for several microseconds to other reactions. Furthermore, spallation neutrons produced by these fast muons can thermalize in the ID and subsequently capture, producing an erroneous delayed

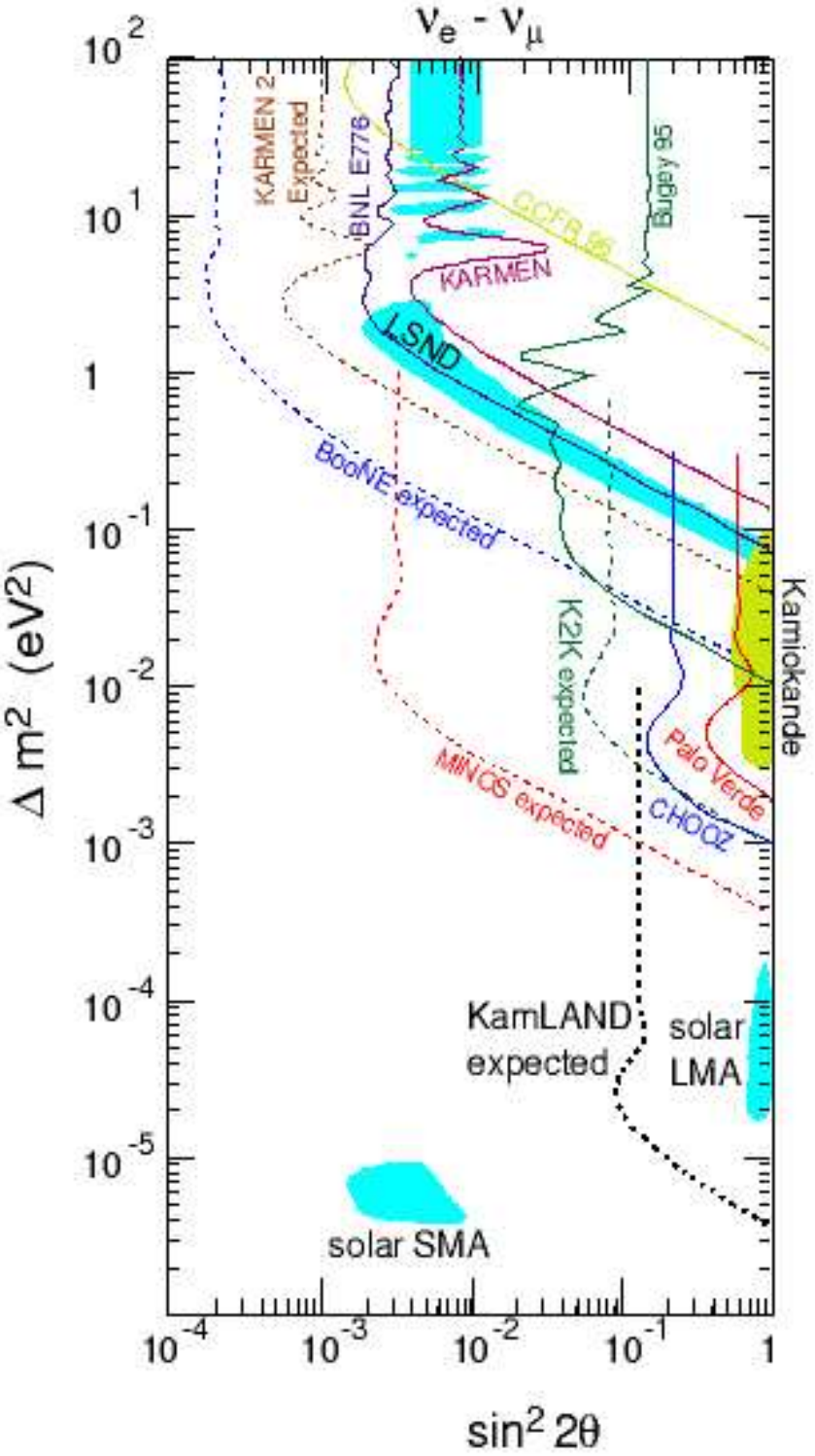


Figure 2.2: Oscillation from $\nu_e \rightarrow \nu_\tau$ as $\delta_m^2$ vs. $sin^2(2\theta)$ showing the sensitivities of several experiments including KamLAND and LMA to the solar neutrino anomaly.

signal. It is the responsibility of the OD to tag muons entering KamLAND to help reduce these backgrounds.

## 2.3 Outer Detector Physics

The OD relies on a phenomenon known as Čerenkov radiation to detect muons at KamLAND. Čerenkov radiation was originally observed as a bluish white light emitted in water shielding nuclear reactors, but was later demonstrated as a more general electromagnetic interaction. Much like scintillation, Čerenkov radiation is a process that any charged particle may undergo, but these particles must travel faster than the phase velocity of light in their propagation medium. Conceptually one may regard the process in much the same way as the wake of a boat results from it moving faster than the propagation speed of waves on the water's surface. In our case however, the effect is most pronounced in dielectric media.

If one considers a particle passing through a dielectric at slow speeds (compared to the speed of light in that medium) the atoms of the surrounding material are readily polarized. In fact, because the particle is moving slowly, the distribution of polarization is spherically symmetric and the corresponding fields at distances far from the polarization interact destructively. If instead the particle is moving faster than the phase velocity of light in the medium, the distortion of the particle's field does not enable atoms ahead of the particle to become polarized. Atoms behind the track are still polarized with azimuthal symmetry, but the general spherical symmetry is gone. Without this symmetry the electric dipole field of the polarized atoms is present even at large distances, and the rapid change in this dipole as the particle passes creates small wavelet emissions. There is an angle called the Čerenkov angle at which all of these wavelets are in phase with one another and create the observed wavefront. Because the dipole still possesses azimuthal symmetry the wavefront will be conical, and the high frequency of dipole oscillation gives the wavefront its bluish hue.

Geometrically, the Čerenkov angle can be computed through a straightforward argument. Denote the velocity of our particle $\beta$ in units of the speed of light $c$, so that in a time $t$ it travels a distance $\beta ct$. During the same interval a wavelet emitted at time zero will have travelled $\frac{c}{n}t$, where $n$ is the index of refraction of the surrounding medium. Since $\beta > \frac{c}{n}$ the two distances form two legs of a right triangle subtended by the Čerenkov angle $\theta_c$. This implies that (see Figure 2.3):

$$\cos(\theta_c) = \frac{1}{\beta n}. \tag{2.7}$$

For the water of the OD a few points are in order. First, as $\beta$ increases, $\theta_c$ increases up to a maximum angle of 41.2 degrees given by the limit as $\beta$ approaches 1 in the equation above. Similarly one can calculate the minimum kinetic energy a particle needs in order to emit Čerenkov radiation in water, $\beta > \frac{1}{1.33}$ which for muons corresponds to an energy of about 55 MeV. At KamLAND the average muon energy is near 220 GeV, roughly four orders of magnitude above this threshold so we will use the maximum $\theta_c$ in our upcoming computations. Finally, the above derivation relies on a constant propagation speed for the particle, which is in general a good assumption, but is even better for KamLAND's energetic muons.

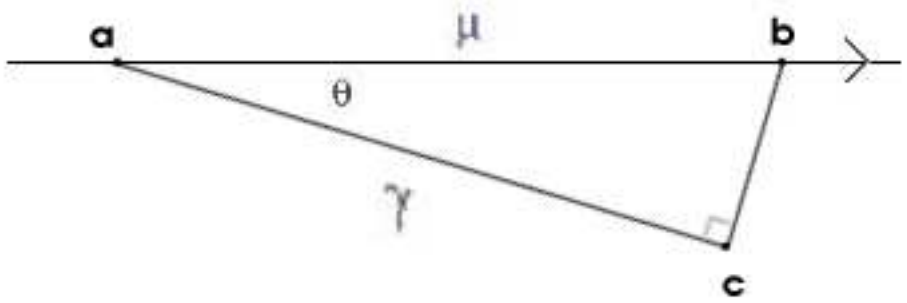


Figure 2.3: Čerenkov radiation is emitted by a muon at point **a**, which travels to **c** in a time $ct/n$. The muon travels a distance $\beta ct$ to point **b**. At points along $\bar{ab}$ radiation will be emitted with the same angle $\theta$, forming a wavefront along $\bar{bc}$.

# Chapter 3

# GEANT Simulations

Monte Carlo calculations have been instrumental to a large extent in data analysis at KamLAND, particularly in understanding data coming from the inner detector. However recent problems with failing phototubes, questions about muonic backgrounds and interest in supporting the inner detector's muon fitter with tracking from the OD (to be discussed in Chapter 4) has put more emphasis on OD simulations throughout the collaboration.

In November of 2001, before KamLAND went into full operation, 23 nonfunctional phototubes in the Outer Detector were discovered. Several had high voltage problems after being submerged in the OD water, resulting in no, or spurious signals. Unfortunately, the number of PMTs which had failed under these conditions did not remain constant. Repeatedly tubes were deactivated based on abnormally high data rates, and by February of 2003 the total number of tubes was down 37% - a consistent loss rate of about 2.1 tubes per month. Perhaps more alarmingly, internal work at TUNL indicated that there was no consistent scheme of tube decay. Tubes failed in each region, sometimes near or far from previously deactivated tubes. Naturally, this raises the question of how many tubes can fail before the OD is no longer useful. Globally it has been demonstrated through Monte Carlo simulations that a muon tagging efficiency at the 95% threshold can be achieved in the event of 165 deactivated tubes, with the remaining 60 PMTs divided evenly among the OD regions [Mes03]. In the

present body of work, we would like extend this study to include regional tagging efficiencies, for direct comparison with studies performed on actual data. For our purposes we concentrate on GEANT3, a Fortran based Monte Carlo program which though older, is more reliable and efficient in our applications, than its most current C++ based version (GEANT4).

## 3.1 Introduction to GEANT and ODsim

GEANT (GEometry ANd Tracking) is a software package that was developed at CERN for the express purpose of modeling the interaction of particles with detectors in high energy physics experiments. Accordingly, the software comes with a robust package of particle definitions, material properties, and physics processes which can accommodate many types of detector. To provide this type of flexibility, the code is not itself a stand alone entity. Instead, the user provides a series of routines specifying all details of a particular experiment to the GEANT kernel. The geometry and material composition of the detector, as well as the individual sensitive elements (photomultipliers, calorimeters, etc.) and their responses to different particles are all defined through these routines. The responsibility of the kernel at runtime is to propagate particles through the detector, passing kinematic and hit information between user functions to simulate the data taking process. GEANT is extremely convenient for the physicist in providing access to particle information and even visualization routines for particles traversing the detector which are not generally available during a real experiment. In this vein, the programmer must be careful to appropriately simulate the detector's response to give meaningful results.

Parameters relevant to the analysis of actual KamLAND OD data can be summarized as follows. $NSUM$ is a number that is used either to specify the total number of phototubes that have fired in a region, or in the entire detector. For instance, the current veto thresholds for muon events are regional $NSUM \geq (6, 5, 6, 7)$. These thresholds have been determined experimentally to trigger the OD at the expected

muon rate, and have been confirmed through simulations [Mes03]. Further, the time a phototube is triggered relative to the event time (taken to be the leading edge of the PMT waveform) and the total charge deposited in that PMT are two other important pieces of information. Each of these has a counterpart in our simulation and will be discussed as we proceed.

In our instance of GEANT, ODsim, KamLAND's geometry has been specified down to the last PMT. The entire detector is then surrounded by one meter of rock to provide a source for rock-born spallation neutrons to KamLAND. A typical muon event in the simulation starts with the generation of a muon and its kinematics, sampled from the known Kamioka muon distribution. Though upward going muons are possible through muonic neutrino interactions in the rock, the majority of real muons are downgoing and are the only ones considered in our simulations. The muon track is started on the edges of detector, and its tracking proceeds in steps calculated by the GEANT kernel based on physics process interaction probabilities and distances to boundary surface interactions. At the end of each step, GEANT records all of the dynamic variables of the track, including any Čerenkov/scintillator generated photons, and passes them to user routine *gustep*. It is here that the programmer specifies how this information is recorded as 'data.' At the end of *gustep*, control is passed back to the GEANT kernel and another step is taken. An event ends when the muon track has stepped its way out of the rock annulus. The kernel then passes control of execution to *guout*, a user routine that has access to the data structures created in *gustep* for finally writing out the collected data. In ODsim, the data is written as an NTUPLE, a histogramming data structure used by the analysis application PAW. The NTUPLE contains information on track kinematics, as well as NSUM values and PMT firing times for each event in an execution of ODsim. We will use *gustep*, *uanal* (a subroutine of *guout*), and the resulting NTUPLE to make our calculations.

## 3.2 ODsim H@X

In order to calculate the efficiency of the outer detector ($E^r$) we need to know the number of muons $N_\mu^r$ traversing each OD region $r$, the corresponding regional NSUM$^r$, and the region's trigger threshold $T^r$. The calculation is straightforward:

$$E^r = \frac{\Gamma_\mu^r}{N_\mu^r}, \tag{3.1}$$

where $\Gamma_\mu^r$ is the number of muons in a region $r$ such that $NSUM^r \geq T^r$. In truth, there are two types of efficiencies. The first is a general efficiency calculation, which uses the internal parameters of GEANT to assign a tag to each muon passing through each OD section. This is not possible in reality, and so corresponds roughly to the idea that in actual KamLAND analysis every muon is tagged, and precisely fit to its genuine trajectory. Hence, this computation provides an estimate of the true detection efficiency provided the simulation is an accurate one. The second type of efficiency mimics the data cuts made when performing an efficiency calculation on real data, and uses a restricted set of information from GEANT. In the actual analysis, a muon fitter based off ID information is used to determine which regions a muon enters. Using GEANT's internal knowledge of track position instead, this computation can be useful in assessing the tracking ability of the ID fitter. Of course, a more beneficial study would use an OD muon fitter for the tracking and will be discussed in Chapter 4. At present, both types of calculation are considered.

Ideally one would like to use as few of the GEANT internal variables as possible to accurately model real analysis. However, to save processing time the full features of the ID portion of ODsim have been disabled and the use of just OD $NSUM^r$s, for instance, is not a sufficient tool for determining a muon's presence in region $r$. In particular, recall that the upper and lower sections of the detector are not physically separated so that reflective properties of Tyvek make it possible for light generated in the upper region to find its way into a lower region PMT. This process may occur even if the muon never enters the lower region.

To tag muons, then, we first exploit the parameters in *gustep* and make a simple tagging algorithm based on the position of the muon, and the material it is propagating through. Since the outer detector is the only place in KamLAND with water, the muon is tagged only when passing through this medium. Note that this takes care of all radial dependences of the detector geometry since the detector is cylindrically symmetric, and leaves only the vertical position of the particle as a free variable. Fortunately, this can be used to determine where in the detector the track falls, since the regions are divided vertically at $(1000 \geq z > 800; 800 \geq z > 0; 0 \geq z > -800; -800 \geq z > -1000)$ *cm*. At each step of the muon's life the code determines which, if any OD region, it's in and passes this information at the end of the event to *uanal*. This routine then adds a new Boolean flag for each of the OD sections to the output NTUPLE. In this way, cuts on presence in each OD section can be made when viewing event histograms.

## 3.3 Computations

The calculations were performed for a variety of dead phototube scenarios utilizing a Perl script written to disable phototubes within the simulation. Each scenario was run with 5000 muon events, and started with the same seeds to the random number generator responsible for particle tracking. We make cuts on the resulting data as follows. By region we cut first on muon presence, and subsequently on $NSUM^r \geq T^r$. Counting the surviving events completes the computation. This can be extended to a global efficiency calculation, following [Mes03] with:

$$E_{global} = \frac{\#Events - \#BelowThreshold}{\#Events - \#RockEvents}, \tag{3.2}$$

where RockEvents are muons which do not enter any region. Note that although each vertex begins on the edge of the simulated KamLAND, not all of the muon momenta point in toward the detector. We further divide the calculation with an additional cut on muons which deposit at least one photoelectron into the ID (indicating presence therein) used to make a rough comparison to actual analysis methods. A represen-

tative sample for scenarios depicting the full complement of OD tubes, the current number of disabled tubes, and 140 randomly disabled PMTs is shown in Table 3.1.

| Scenario/Region | Bottom | Lower | Upper | Top |
|---|---|---|---|---|
| **0 Dead Tubes** | | | | |
| Idpe | 99.4% | 98.8% | 98.8% | 95.1% |
| All Events | 98.9% | 98.8% | 99.0% | 96.3% |
| Global | 99.3% | | | |
| **Current OD** | | | | |
| Idpe | 98.3% | 98.5% | 97.7% | 94.5% |
| KamLAND Cuts | 97.7% | 100% | 100% | 93.1% |
| KamLAND Results | 82.6% | 99.9% | 99.9% | 93.3% |
| All Events | 97.2% | 98.5% | 98.4% | 95.6% |
| Global | 98.7% | | | |
| **140 Dead Tubes** | | | | |
| Idpe | 96.1% | 96.2% | 90.0% | 89.5% |
| All Events | 94.9% | 95.9% | 91.7% | 89.2% |
| Global | 97.7% | | | |

Table 3.1: Efficiency calculations globally and by region for three different dead PMT scenarios: none dead, the real number of dead tubes, and 140 randomly disabled tubes. Calculations are further divided into muons which went through the inner detector (Idpe), and all events. For the current dead tube status of KamLAND, a final calculation using real analysis data cuts is shown for both real (KamLAND results) and simulated data (KamLAND Cuts).

A final computation is made to compare simulation studies with real data analysis. Because KamLAND does not have the luxury of knowing the exact trajectory of each passing muon, tagging muons by region is done using a fitter which collects time and charge information from the ID. Since there is at the time of writing, no

fitting algorithm based on OD parameters, muons which do not enter the ID are never considered. Accordingly the 'All Events' computation listed in Table 3.1 is the "expected efficiency" of the OD in the event all muons in the detector cavity could be tracked. In a similar fashion, the 'Idpe' computation is the "expected efficiency" if all ID going muons were perfectly detected and tracked by the current fitter. To compare with real data efforts, we must go one step farther since some muons are more difficult to detect in the ID than others.

If one plots the logarithm of total charge collected in the ID, there are two pronounced peaks for muon like events. The first of these occurs in the real data between $1 \times 10^3$ and $2 \times 10^5$ charge units and corresponds to muons which pass through the inner detector buffer oil region leaving only Čerenkov light. A second peak above $2 \times 10^5$ represents muons which deposit light in the scintillator. It is this former peak which gives KamLAND the most trouble, since unlike their scintillator traversing counterparts, muons in the buffer oil leave considerably less light and resemble other background sources. At the same time, though, they are just as capable of creating spallation neutrons which may travel into the detector's fiducial volume and give a false capture event. Figure 3.2 illustrates the distribution of ID light for Monte Carlo muons.

To test the OD using real data, cuts are made as follows. For the Top (Bottom) regions, the ID muon fitter must place a track in the Top (Bottom) region and deposit more charge than $2 \times 10^5$ units. For the Upper and Lower regions, the track must be fit to both the Top and Bottom sections, and it must go through the buffer oil according to the Čerenkov peak on the ID charge plot. Again, a further cut on the $NSUM^r$ is made and the efficiency calculation is performed in the same way. Results of these cuts for real and simulation data are shown in Table 1.1, and the corresponding $NSUM$ distributions in Figure 3.3.

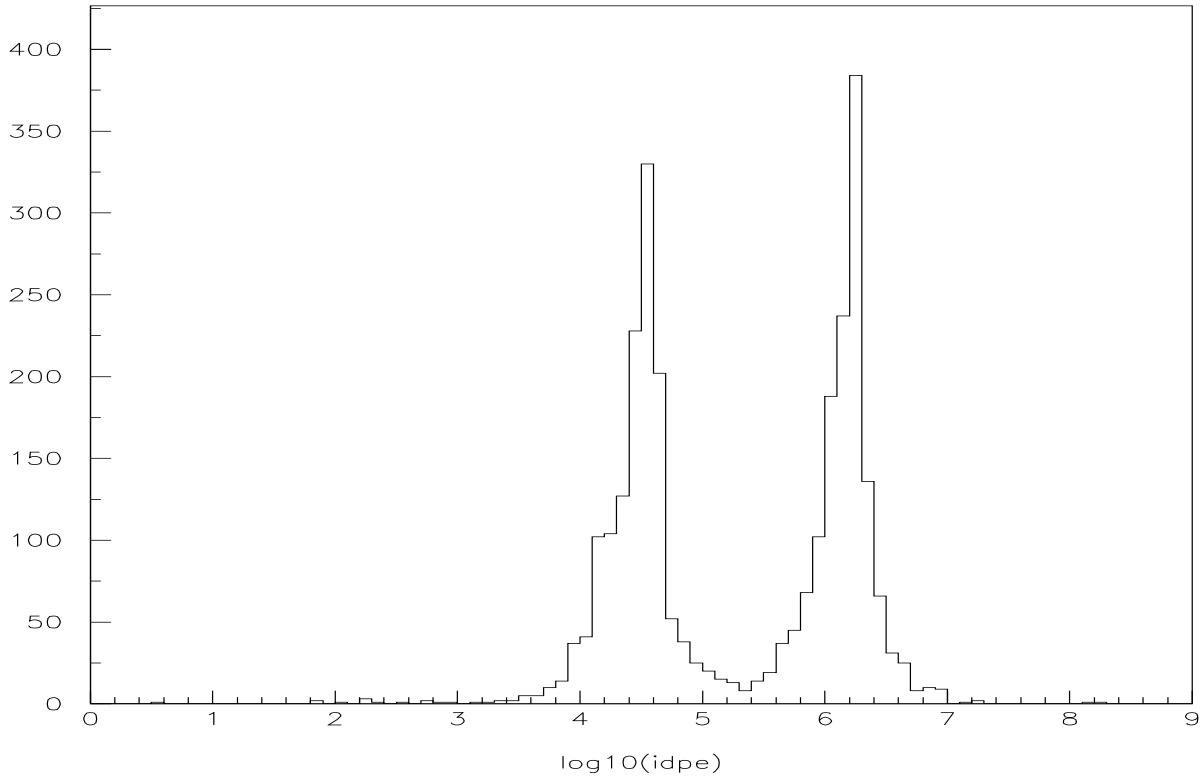


Figure 3.1: $\text{Log}_{10}$ plot of the number of photons deposited in the ID. The first peak corresponds to muons which go through only the buffer oil, and the second contains muons which went into the scintillator as well.

## 3.4 Analysis

A few points standout in the results above. First it has been estimated measurements at KamLAND will be successful if the global efficiency of the OD is at or above 95%. Fortunately, even in the event of a 60% reduction in PMTs our simulations suggest the KamLAND OD will operate above this threshold, a result consistent with [Ref Mess.]. This is not entirely surprising if one considers the regional efficiencies are all near or above 90% in each of the simulations. Indeed one can verify that the muons which fall below each $NSUM^r$ threshold enter at most one region. Of course one would prefer that each of regional efficiencies was at or above the 95% threshold so that each section stands alone as a veto, but the combination of two or more is sufficient.

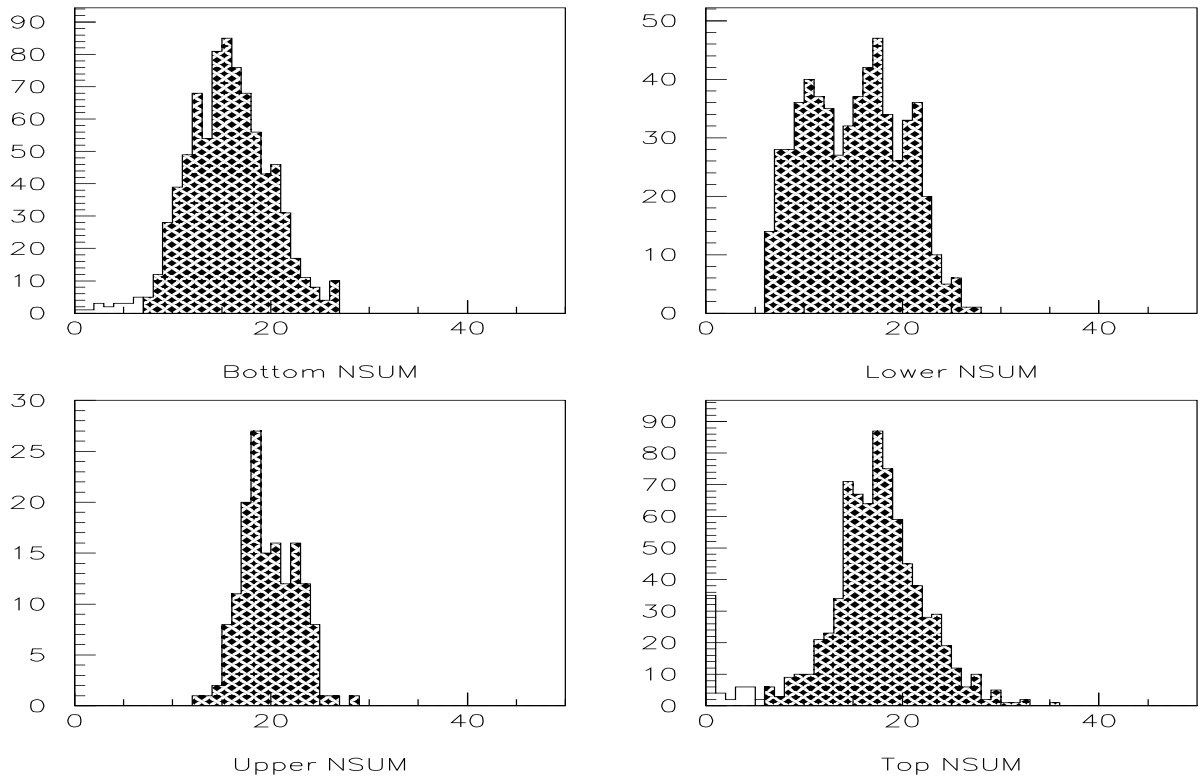


Figure 3.2: $NSUM$ distributions by region for real data analysis cuts using Monte Carlo data. The cross hatched portions denote muons which were above the trigger threshold for that region, and the clear regions are muons below threshold.

It's further interesting that the results for the KamLAND cuts are so near 100% efficiency in the Upper and Lower regions for both real and simulated data. However, this cut geometrically selects muons which go through both regions, so the pool of muons used in the calculation for each region is the same. Since they leave a lot of light in the ID KamLAND's geometry suggests that these muons also spend a lot of time, and hence leave a lot of light, in the OD. Accordingly the efficiency for detecting these muons is high in each region, and the two should be close to the same value.

Note also that the efficiencies for both real and simulated data for the Top region are in good agreement, while there is a considerable difference for Bottom. This latter discrepancy is difficult to resolve since KamLAND does not have access to all properties of the muons it observes, but it can be partially resolved by a comparison of $NSUM$ distributions. Figure 3.3 lists the $NSUM$ distributions corresponding to the

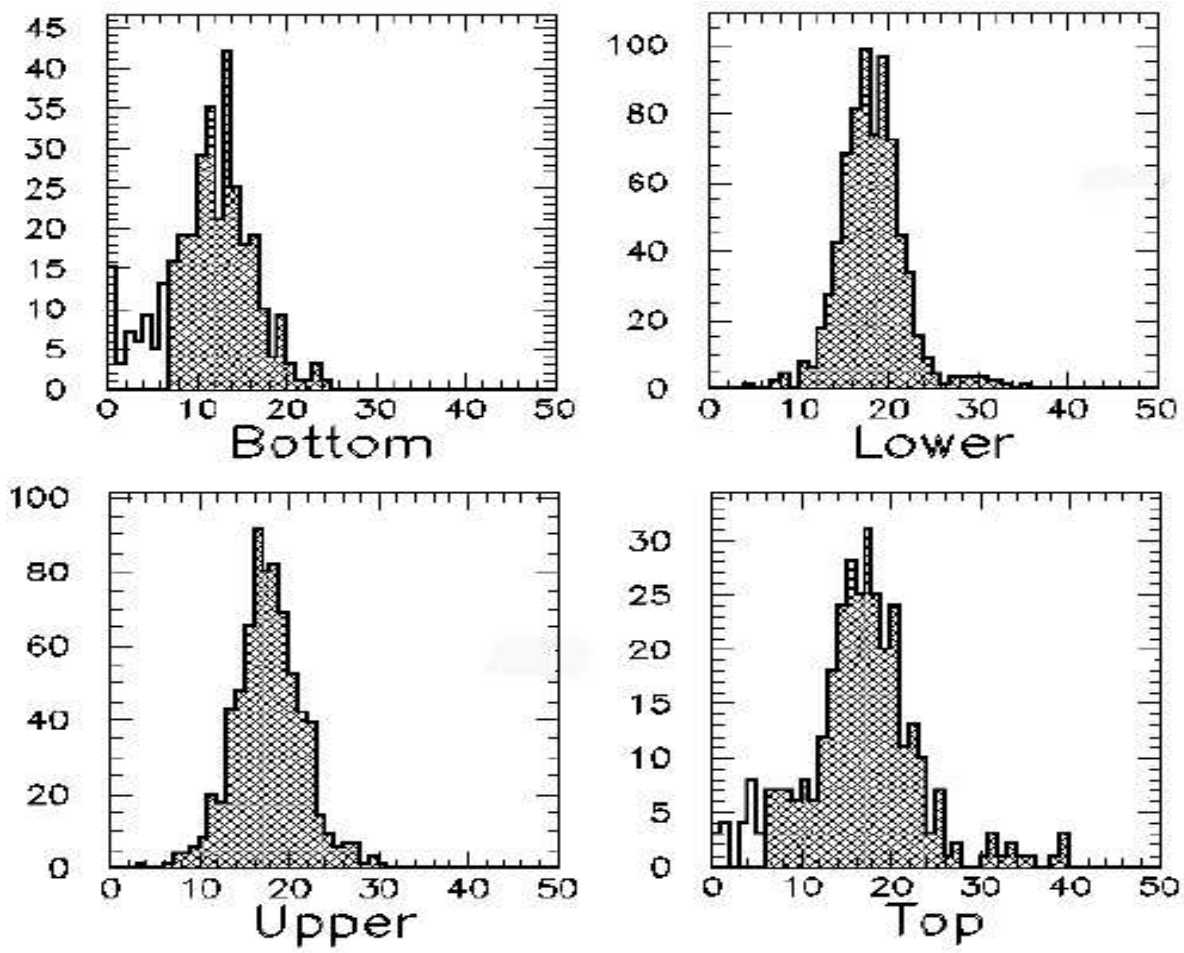


Figure 3.3: NSUM distributions by region for real data analysis cuts using real data.

efficiency calculations of Table 1 for real data. One notices immediately that the real distribution for Bottom has many more events below threshold than the simulated distribution, although each has approximately the same shape, peak position, and maximum $NSUM$ value. Specifically, there are several events at $NSUM = 0$. Since the muons in consideration tend to leave a lot of light, the presence of this spike suggests that some muon tracks in this sample did not actually enter into the bottom region. This is in fact possible since the ID muon fitter has an associated error on the order of 20 cm for track fitting. However, it fits muons to line segment tracks, and since we do not observe a similar spike in Top's distribution, this cannot be the sole reason for the disparity.

Instead, one may notice that there is a spike at zero in the simulation's Top distribution. Each of the events in this spike (and all of the below threshold tail) began either at the very bottom of Top, or near the ID chimney. In both cases, the muon spent only a small amount of time in the Top region. It is reasonable to assume that many of the below threshold events for the real distribution were similar muons. The absence of a similar peak at zero $NSUM$ would suggest muons may have been incorrectly assigned to a different region (Upper) by the ID fitter.

# Chapter 4

# OD Muon Tracking

As proposed in the previous chapter, it is possible that the ID muon fitter does not track muons with sufficient accuracy to account for the discrepancy seen in calculations performed with simulation data. Developing an OD muon fitter to complement the ID serves many purposes. As an alternative to using GEANT's internal routines to determine which OD regions a muon enters, an OD fitting algorithm may give a better idea about the sectional efficiencies as seen by fitting routines. That is, performing the calculations of Chapter Three again may give results more similar to the real analysis. Further, if an algorithm is developed then both fitters can work in concert to give a more accurate result and reduce errors found in either algorithm by itself. This of course leads to better background reduction, the principal goal of the OD.

Creating a muon fitter is in general a difficult problem since a muon in either the scintillator or in Čerenkov processes will emit light all along its path. The timing and charge distributions of PMTs viewing the event are accordingly some averages of vertex-like events taken all along the track. Not knowing where to place each of these vertices makes computing timing cuts, for instance, more difficult. The problem is compounded in the outer detector because the Tyvek found throughout reflects light, trapping it in the OD. While this trapping is good for general veto purposes, after a photon reaching a phototube has been reflected many times, one cannot easily

determine where it was created; a straight line path for such a photon drawn from the PMT would end on a surface. This is particularly difficult in cases where light reflects off the ID sphere.

To surmount this difficulty we again appeal to Monte Carlo simulations. Our hope is that through careful analysis and repeated execution of simulation data cycles various correlations between parameters will become apparent. Ideally, we would like to investigate the relationship between the distance of closest approach to a PMT and the amount of light it sees relative to its neighbors. To begin with we shall consider the Upper and Lower sections of the OD, since the PMTs in these regions are organized in rows (the Top and Bottom PMTs are organized radially) and their data may therefore be easier to understand. With this in mind our goal is to develop a fitter for each region separately, and have their independent fits agree on simulated muon tracks at the boundary between them. This boundary matching criterion will be later used to test new algorithms for the remaining two regions.

## 4.1 Methods

In order to search for patterns *gustep* and *uanal* were again modified. *Gustep* provides the programmer with the current step's time of flight since the particle's creation. For muons, this number represents the time since the start of the event. Each Čerenkov photon produced is associated to the time of flight for its parent muon at the photon's creation. The average of all these times for photons in a given phototube is written to our NTUPLE as the firing (event) time for that phototube. In a similar fashion, the number of photons reaching a tube is also recorded and serves as the charge deposited in the PMT. Roughly speaking, in real data situations these are the only variables at our disposal. Our final algorithm therefore should only rely on time and charge information from the OD PMTs.

In *uanal* we added distance calculations to the data output. Using the initial vertex kinematics in the routine, we can compute the distance of closest approach as well as the planar distance to any PMT, assuming the muon follows more or less a straight line path. Since our first efforts concentrate on the Upper region, an arbitrary Upper PMT was chosen as the focus of the algorithm studies. The charge, event time, distances, and impact parameter angles have been included in the simulation data for the main tube as well as its nearest, and next nearest neighbors.

When looking for patterns the initial search often involves some form of Fourier transform. For ODsim, a Fourier transform for a single event's charge distribution by PMT gives a mode at 20 PMTs. Unfortunately, this frequency corresponds to the periodicity of phototube numbering within ODsim, and not to any otherwise useful behavior. The PMTs of the Upper (and Lower) come in three rows of 20 tubes each along the circumference of the OD. PMTs separated by 20 numbers share the same azimuthal location, but the difference in their verticals is 200 cm.

Though it might be convenient to utilize this periodicity in our fitting program, one has to be very careful about its implementation. If, for instance, only exactly vertical-going muons are considered, one can assume that the light seen by an Upper PMT is emitted at the maximum Čerenkov angle from its track. This will certainly be true for light that is not reflected before it reaches the tube. Unfortunately though, simulations indicate that neither the event time, nor the charge in a given PMT, are even roughly the same when viewing the same muon. In fact, Figure 4.1 illustrates that both parameters have a near Gaussian form for the same muon event run one thousand times. The peaks of the distribution are not sharp enough to permit one to create an algorithm associating a particular event time with path length for photons emitted at the Čerenkov angle. All of this indicates that our algorithm will likely involve taking samples of random variables created from simulations as input parameters.

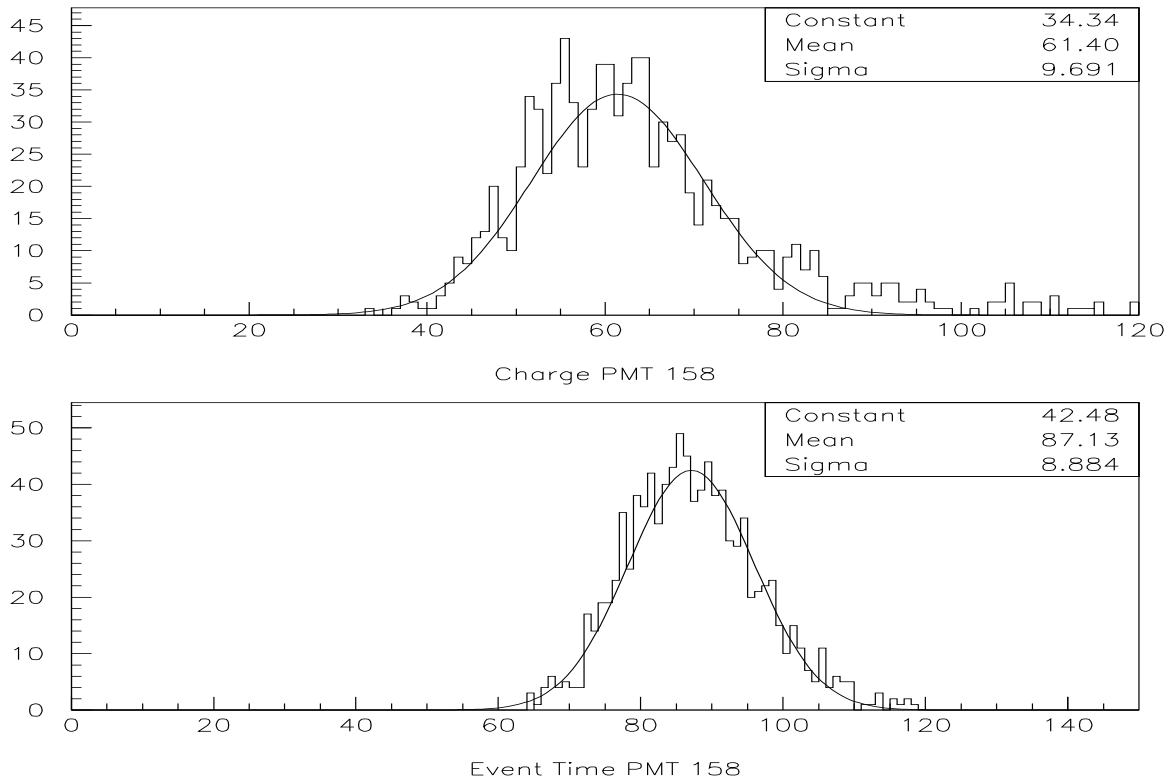


Figure 4.1: Time (ns) and charge (photon counts) distributions and fits to Gaussians for PMT #158, for 1000 events run with the same starting position, impact parameter and momenta. The perpendicular distance of this track to the PMT was chosen to be 35 cm.

With this in mind, our next procedure is to determine if a distance associated to a PMT can be used to set limits on kinematic variables based on features of the resulting output data. To do this, the generator responsible for drawing particles from the Kamioka muon distribution has been modified to sample all muons, but only track those which will pass through a given point. The chosen point is 35 cm from PMT #138 in the perpendicular plane of its vision, and we run 5000 muon events with their only common parameter being a trajectory that includes this point. Since our previous work suggests that similar photon tracks do not leave consistent amounts of light in any given phototube, we will consider only the percentage of total charge accumulated in a tube as compared with its nearest in-plane neighbors.

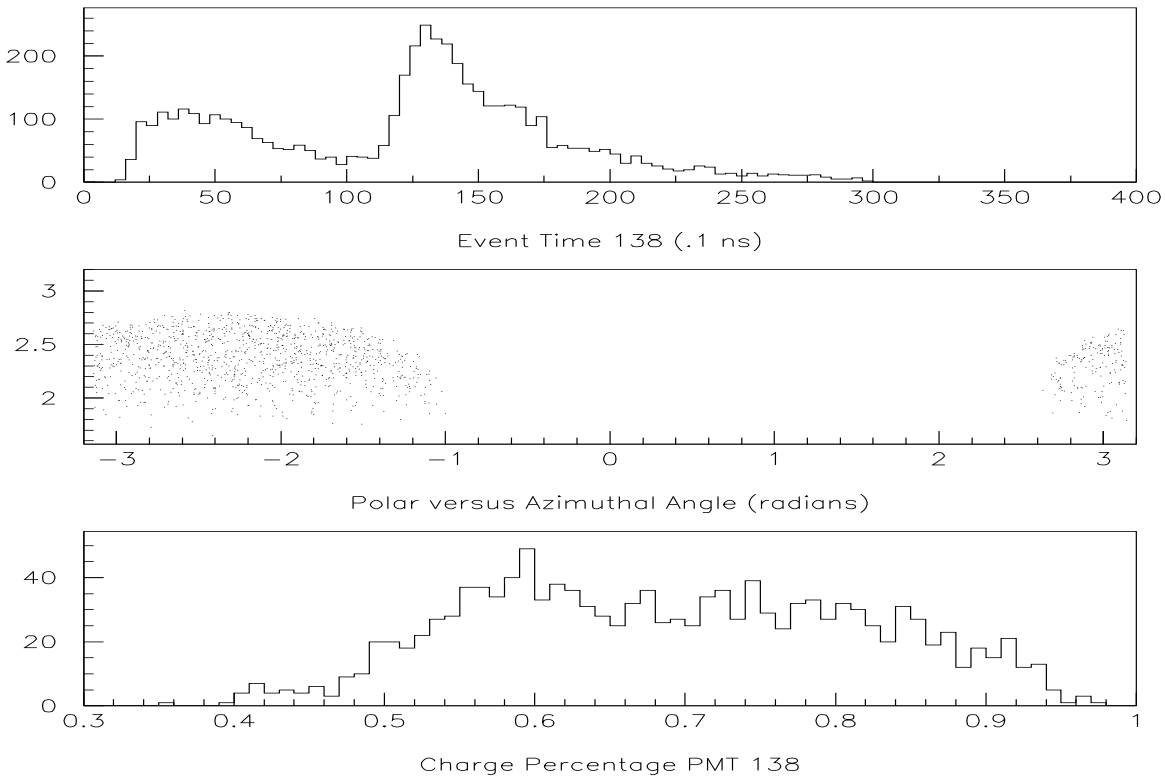


Figure 4.2: PMT #138 plots. The first plot shows the event time distribution for 5000 events run through a common point. The next plot shows the region in impact parameter space occupied by muons with event times less than 7.5 ns, and the final distribution is the charge percentage seen for those same muons.

For these events, the Gaussian shape of the event time distribution for our focus PMT and its nearest neighbors is removed. Instead there are two pronounced peaks as illustrated in Figure 4.2. Fortunately some information can be gleaned by examining the parameters associated with these peaks. It can be shown that events occurring in first peak only started on the OD outer cylinder (not the ceiling) between azimuthal angles 18.7° above and below the azimuthal angle of the target PMT. The impact parameters (polar versus azimuthal momentum direction) of these muons are also confined to a circular region of this space. Further, the large majority of these originated in Upper and a small amount started near the boundary between Upper and Top. To make these statements into useable cuts we note that the charge in the target exceeds 50% of the total charge in surrounding tubes for the bulk of these events, and is always greater than 40% (see Figure 4.2). While this is a large step in the correct

direction, we are associating regions in the data space to regions in kinematic space, and not points to points.

If instead we focus on the second peak in the timing distribution of Figure 4.2 we can illustrate how we may be able to constrain regions of the impact parameter space to construct an algorithm. Consider the timing distributions in Figure 4.3, for PMT #158, #118 and #98, positioned 200cm above, 200cm and 800cm below #138, respectively. Note that the second peak described above shifts towards later event times as one views the plots in decreasing PMT number. This is as one would expect for down going muons. Consentrating on the impact parameters for light entering PMT #138 with event times between 12 and 16 ns yields a very interesting shape. Portions of that shape may be peared by cutting again on muons which produce light in PMTs #158 and #118 within their second peaks: 10-14 ns and 18-22 ns (see Figure 4.3). Again, to turn these into potentially useable cuts the final image in Figure 4.3 shows the charge percentage in #138. Note that it has a gently peaked Gaussian character. Further note that based on our observations on the first timing peak, a charge percentage within this Gaussian is not alone a sufficient condition for constraining the impact parameter.

Clearly several problems remain with this approach. The method is very complicated in that a vast number of statistics are necessary to accurately model the muon's progress. In addition, the difficulty in applying many cuts on the same data set corresponding to different features from neighboring PMTs is that the number of surviving events decreases. Finally, these results are really only valid for muons which pass through the point specified above, something KamLAND will not have knowledge of ahead of time. Although there is still much work to be done to create a complete algorithm it is hoped that further considerations will enable tighter limits on available regions in our parameter spaces.

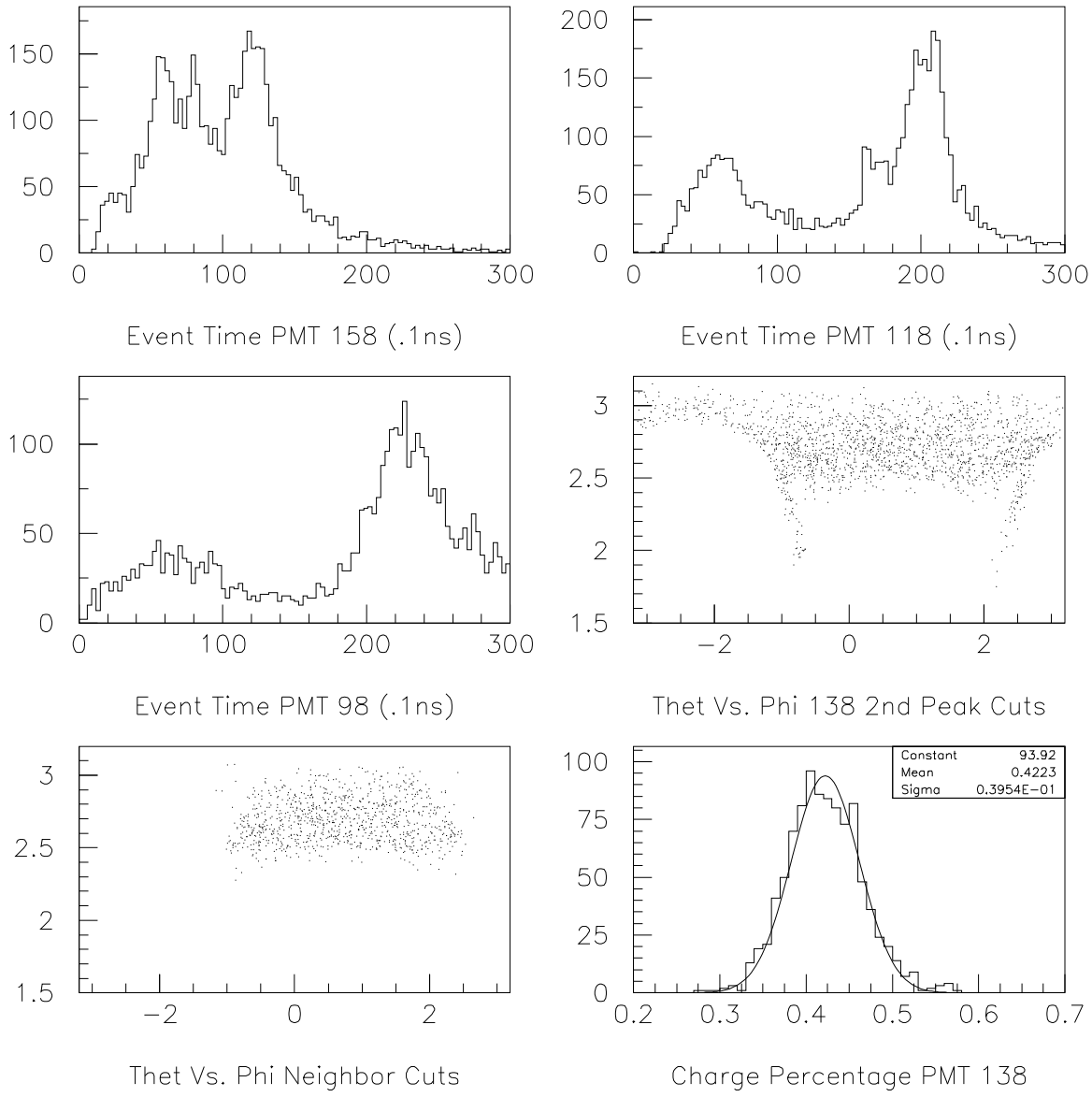


Figure 4.3: From top left: Event timing distributions for three PMTs one directly above and two below PMT #138. The fourth image is the impact parameter space for muons cut on times within the 2nd peak of PMT #138's timing distribution (see Figure 4.2), followed by the same plot for cuts on event times with the 2nd peak of PMT #138's neighboring PMTs. Finally, the charge percentage distribution of PMT #138, fit to a Gaussian for these cuts.

# Chapter 5

# Conclusions

KamLAND's first results measured a ratio of observed to expected antineutrinos at energies greater than 3.4 MeV of $0.611 \pm 0.085(\text{stat}) \pm 0.041(\text{sys})$, confirming not only neutrino oscillations, but also isolating the Large Mixing Angle solution to the solar neutrino problem[Egu03]. This result was supported by many efforts throughout the collaboration to reduce muon induced background signals. The next phase of KamLAND requires even tighter constraints on backgrounds and so these efforts continue.

In order to test the muon transport of KamLAND GEANT implementations, one study aims to create and track muons from beyond Mount Ikenoyama through the detector with another program, MUon SImulation Code (MUSIC). The advantage of using MUSIC over GEANT is its faster propagation routines through media such as the surrounding rock. This study has been able to confirm, using the mountain's geometry, the observed muon rates and impact parameters at the Kamioka site. Another study focuses on removing erroneous muon events from the data pool that are created by noisy OD PMTs, or ringing in upgraded electronics using information from the ID. Finally, efforts to improve the accuracy of the ID muon fitter using advanced light propagation models in the liquid scintillator are an ongoing project.

It is the aim of our studies to integrate with these efforts and form a rigid background reduction programme at KamLAND. Our simulations have indicated that the sectional OD efficiencies are above the necessary global 95% threshold for the current KamLAND disabled PMT scenario. Further, for three regions in this scenario, efficiencies using real data analysis cuts on Monte Carlo data are in good agreement with those performed on actual data. That is, the prescription used on real data yields reasonable numbers. This knowledge will later serve to increase confidence in current background elimination methods.

Finally, the analysis of Monte Carlo data suggests that it is possible to create a muon fitting algorithm based upon only OD event information. That this fitter will likely have to implement an abstract method of successively narrowing regions in parameter space is not surprising, considering the reflective abilities of the OD Tyvek. The development of this algorithm is driven by a need to improve the accuracy of muon fits from the ID. If the OD algorithm can be made to consistently agree with the ID muon fitter, cylinder cuts made around a muon's track can be tightened. Tighter cuts will give a better indication of regions along the muon's trajectory where spallation signals are possible, and thereby reduce detector blind time.

# REFERENCES


[Ahm02] Q. Ahmad et al., "Direct Evidence for Neutrino Flavor Transformation from Neutral-Current Interactions in the Sudbury Neutrino Observatory", Phys. Rev. Lett. **89**, 011301 (2002).

[Bah98] J. Bahcall, P. Krastev, and A. Smirnov, "Where Do We Stand with Solar Neutrino Oscillations?", Phys. Rev. D **58**, 1 (1998).

[Egu03] K. Eguchi et al., "First Results from KamLAND: Evidence for Reactor Anti-Neutrino Disappearance", Phys. Rev. Lett. **90**, 021802 (2003).

[Fuk98] Y. Fukuda et al., "Measurement of the Solar Neutrino Flux from SuperKamiokande's First 300 Days", Phys. Rev. Lett. **81**, 1562 (1998).

[Giu03] C. Giunti, "Theory of Neutrino Oscillations", in *11th Lomonosov Conference on Elementary Particle Physics, 21-27 August 2003, Moscow State University, Moscow, Russia*, 2003, See hep-ph/0401244.

[Hir88] K. Hirata et al., "Observation in the Kamiokande-II detector of the neutrino burst from supernova SN1987A", Phys. Rev. D **38**, 448 (1988).

[Kay00] B. Kayser, "Neutrino Mass, Mixing, and Oscillation", in *Proceedings of TASI 2000*, 2000, See hep-ph/0104147.

[Mes03] J. Messimore, *The KamLAND Outer Detector*, Ph.D. thesis, North Carolina State University, 2003.